www.vbripress.com/aml, DOI: 10.5185/amlett.2016.6457 Published online by the VBRI Press in 2016

Study of A-site divalent doping on multiferroic properties of BFO nanoparticles processed via combustion method

Baljinder Kaur[1,2,3], Lakhbir Singh[1,2,3], V. Annapu Reddy[4], Dae-Yong Jeong[5], Navneet Dabra[6*], Jasbir S. Hundal[2]

[1]*Yadvindra College of Engineering, Punjabi University Guru Kashi Campus, Talwandi Sabo 151302, Punjab, India*
[2]*Materials Science Laboratory, Department of Applied Physics, Giani Zail Singh Campus College of Engineering & Technology, Maharaja Ranjit Singh Punjab Technical University, Bathinda 151001, Punjab, India*
[3]*Research Scholar of I.K. Gujral Punjab Technical University, Near Pushpa Gujral Science City, Kapurthala 144603, Punjab, India*
[4]*Functional Ceramics Research Group, Korea Institute of Materials Science (KIMS), Gyeoungnam 641831, Korea*
[5]*Department of Materials Science and Engineering, Inha University, Incheon 402751, Korea*
[6]*Mata Sahib Kaur Girls' College (affiliated to Punjabi University Patiala), Talwandi Sabo 151302, Punjab, India*

[*]Corresponding author. E-mail: navneetdabra@gmail.com

Received: 02 February 2016, Revised: 14 February 2016 and Accepted: 22 June 2016

ABSTRACT

Pure and Sr-doped bismuth ferrite $Bi_{1-x}Sr_x$ FeO_3 (x = 0, 0.1, 0.2, 0.3) nanoparticles have been synthesized using combustion method. X- Ray diffraction study of these compounds confirms the rhombohedral structure with R3c space group. $BiFeO_3$ peaks were observed at 2θ = 22.46º, 31.80º, 32.11º, 39.519º, 45.79º, 51.35º, 56.98º and 57.16º having miller indices as (012), (104), (110), (202), (024), (116), (214) respectively. The traces of secondary phase also appear along with desired phase of Sr-doped bismuth ferrite $Bi_{1-x}Sr_xFeO_3$ samples. The scanning electron microscopy of fractured pellets of the samples reveals the decrease in grain size with increase of Sr doping in $Bi_{1-x}Sr_xFeO_3$. Magnetic studies were carried out at room temperature up to a field of 10 kOe. M-H hysteresis loops showed a significant increase in magnetization with Sr substitution in $BiFeO_3$. Compared to weak magnetisation with magnetizing field (M-H) shown by $BiFeO_3$ nanoparticles (Remnant magnetization, $M_r \sim 0.4x10^{-3}$ emu/g and coercive field, $H_c \sim 0.065$ kOe respectively), a significant enhancement in M-H loop was observed in $Bi_{1-x}Sr_x$ FeO_3 compounds. The value of $M_r \sim 0.525$ emu/g and $H_c \sim 3.70$ kOe have been found to be maximum for x = 0.30 in $Bi_{1-x}Sr_x$ FeO_3 compounds. Leakage current studies showed decrease in leakage current density of doped samples to that of pure $BiFeO_3$ and x = 0.10 gives minimum value of 4.78 x 10^{-6} A/cm^2 at 350 V/cm. The ferroelectric nature was confirmed by observed P-E loops in all the samples. Copyright © 2016 VBRI Press.

Keywords: $BiFeO_3$; multiferroic; combustion method; XRD; SEM; VSM.

Introduction

The field of multiferroics has attracted wide interest of researchers, as these have vast prospective for the conception of magnetoelectric and magneto-optical devices **[1-2]**. The peculiar exhibition of coexistence of ferromagnetism, ferroelectricity and / or ferroelasticity by multiferroic materials in a certain range of temperatures has engrossed much interest **[3]**. These materials could produce electrical polarization by applying external magnetic field; alternately magnetization could be induced by an external electric field. Multiferroic materials can provide wide avenues for impending applications in ferroelectric as well as magnetic devices **[4-6]**. Therefore, such materials based devices can be put in three categories: the devices that employ magnetic and ferroelectric properties exclusively; the devices simultaneously employing ferroelectric and magnetic properties but without magnetoelectric interaction and the devices which rely on the magnetoelectric effect **[7]**. This coupling opens extra degrees of freedom in the materials which enable a control on the magnetic properties by applying an outer electric field and vice-versa, providing a possibility to develop new devices based on these materials.

$BiFeO_3$ has engaged much attention of researchers among the class of multiferroic materials by exhibiting wide potential applications in the area of spintronics, electromagnetic coupling, data storage devices, sensors, and permanent magnet **[8-12]**. $BiFeO_3$ displays coexistence of ferroelectric and anti-ferromagnetic ordering in a single phase at room temperature, that is, applied magnetic field can control electric properties and by varying electric field the magnetization can be controlled **[13]**. $BiFeO_3$ has been considered as the genus multiferroic oxide with distorted rhombohedrally perovskite structure having space group R3c **[14]**. It has room temperature multiferroic features

having ferroelectric (Curie temperature T_C = 1103 K) as well as G-type anti-ferromagnetic (Neel temperature T_N = 643 K) properties **[15]**. In pure $BiFeO_3$, ferroelectricity appears as the $6s^2$ lone pair of Bi^{3+} ions causes off centred distortion of Fe^{3+} ions to give it non-centrosymmetric rhombohedral structure **[16]**. The canting of spin structure of $BiFeO_3$ produces localized anti ferromagnetism which is subsequently suppressed at macroscopic level due to its spiral spin structure **[17]**.

In the single phase $BiFeO_3$ ceramics the enhancement of the magnetic properties has been found by doping of both trivalent rare earth elements such as (La, Nd, Er, Y etc) and divalent second group elements (Ca, Ba, Sr etc) on A-site (Bi site) **[18-19]**. Doping of transition metal elements like Ni, Cr, Mn, Ti, Zr etc on B site (Fe-site) has also improved the magnetization value **[20-22]**. It has been reported that (anti-ferromagnetic) ordering could be transformed into a ferromagnetic by reducing the particle size to a nano-scale, subsequently by improving the magnetic properties **[23-24]**. The researchers have been focussing to tailor and enhance the multiferroic properties of $BiFeO_3$ and its related materials in the form of composites, heterostructures and multi-layered structure **[25-28]**.

In the present study, synthesis of $Bi_{1-x}Sr_x$ FeO_3 (x = 0, 0.1, 0.2, 0.3) is done by combustion method in which metal nitrates act as oxidizers and citric acid acts as fuel **[29]**. The stoichiometric fuel to oxidizer ratio was calculated as illustrated by Jain *et al* (1981) **[30]**. The wide applicability range and simplicity are the foremost advantages of using combustion method technique. This method is also advantageous as far as the self-purifying attribute and the possibility of obtaining products in the required size and shape is concerned. Also various parameters of products viz. composition, structure, homogeneity, and stoichiometry can be controlled and homogeneous distribution of the dopant could be achieved all over the host material due to the mixing of the reactants at atomic level in the initial solution **[31]**. The lower costs of preparation due to simple equipments for this easy and fast makes it economically viable in comparison with conventional synthesis methods. In this present work, the substitution of Sr^{2+} ion for Bi^{3+} ion has been chosen for its greater ionic radius (1.26 Å) compared to Bi^{3+} (1.17 Å). The internal chemical pressure generated by Sr^{2+} ions will considerably affect the distortion in structure. This distortion virtually may improve the corporal properties of the system. The structural, electric and magnetic properties of $BiFeO_3$ doped by Sr at Bi site have been investigated. We observed remarkable variations in structural and magnetic properties with increase in Sr content and discussed their origin.

Experimental

Polycrystalline $Bi_{1-x}Sr_x$ FeO_3 (x=0, 0.1, 0.2, 0.3) nanoparticles have been prepared by a combustion method using metal nitrates which act oxidizer and citric acid acts as fuel in the absence of any solvent. Bismuth nitrate ($Bi(NO_3)_3.5H_2O$), ferric nitrate ($Fe(NO_3)_3.9H_2O$), strontium nitrate ($Sr(NO_3)_2$) and citric acid ($C_6H_8O_7$) from 'SD Fine-Chem limited' (SDFCL), Mumbai (India) with purity 99.9% have been used in the synthesis process. Stoichiometric amount of these compounds were heated at 80°C on a hot plate with constant stirring to get a homogeneous gel. Then, the gel was heated at 150°C for combustion to form the precursor which was grounded to fine powder and annealed at 600°C for 2 hours in high purity alumina crucibles in air and then allowed to cool down. Then it was further grounded to fine powder.

Small amount of the finally obtained powder was characterized by X-ray Diffractometer (XRD) (Panalytical X'Pert Pro) with Cu source wavelength $K_{\alpha 1}$ =1.5406Å. Crystallite size was calculated from XRD peaks using Scherrer formula **[16]**. To study microstructure of the samples, Scanning Electron Microscopy was done using SEM machine (JEOL made). Magnetization data was taken at room temperature using a vibrating sample magnetometer Model PAR 155, from Princeton Applied Research, UK with applied field range of 10 kOe.

The samples in the form of a pellet were made using hydraulic press, which were further sintered at 600°C for 2 hours and then polished. The metal contacts of silver were deposited on the flat surface of the pellet using silver paste. Leakage Current Measurements were performed using Agilent B2901 Source Meter Unit. The ferroelectric response of the samples has been studied using Polarization-Electric field (P-E) loop tracer manufactured by Marine India, New Delhi, India.

Results and discussion

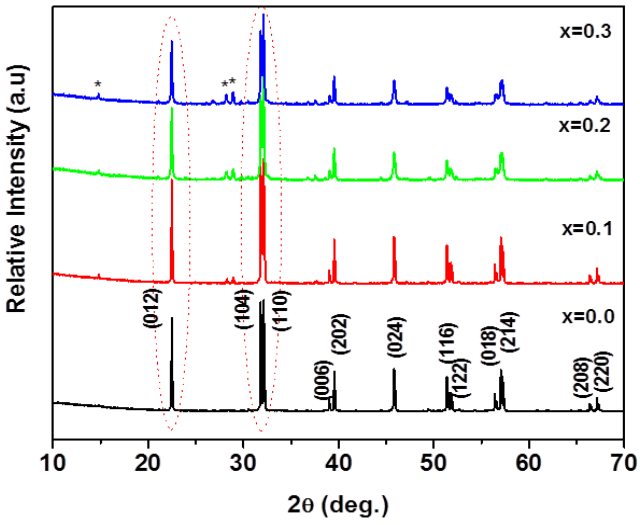

Fig. 1. XRD images of all samples of $Bi_{1-x}Sr_x$ FeO_3 (x = 0, 0.1, 0.2, 0.3) (asterisks * indicate peaks of $Bi_2Fe_4O_9$)

Structural studies

The XRD patterns of all the prepared samples were analyzed. In XRD pattern of $BiFeO_3$ and doped $BiFeO_3$ peaks were observed at 2θ = 22.46°, 31.80°, 32.11°, 39.519°, 45.79°, 51.35°, 56.98° and 57.16° **(Fig. 1).** The miller indices (h k l) of the ensuing planes of $BiFeO_3$ and doped $BiFeO_3$ were matched with the standard pattern of $BiFeO_3$ and are indexed in Figure 1 (JCPDS data 1998, File no. 86-1518) **[32]**. The matched (h k l) values suggest that $BiFeO_3$ has rhombohedral perovskite structure having space group R3c at room temperature **[32]**. Strontium

doping did not cause a change in structure as no new peaks corresponding to any phase associated with Sr were observed. These observations indicate the incorporation of Sr ions into the BFO structure. Weak secondary phase peaks like $Bi_2Fe_4O_9$ were observed along with main peaks. These phases are usually observed in BFO and substituted BFO samples because of the kinetics of formation **[20]**. The peaks of $Bi_2Fe_4O_9$ (secondary phase of bismuth ferrite) having miller indices (h k l) as (121), (211), (001) at $2\theta = 14.80^0, 28.17^0, 28.90^0$ appeared in the doped samples of $Bi_{1-x}Sr_x$ FeO_3 (x=0, 0.1, 0.2, 0.3). The order of increase in peak intensities in these secondary phases follows the order of increase of Sr doping concentration in $BiFeO_3$. This limits further doping of Sr in $BiFeO_3$ **[7, 33]**.

The crystallite sizes of all the samples were obtained from the diffraction peak having maximum intensity in the pattern using Scherer's formula. The crystallite size of $Bi_{1-x}Sr_x$ FeO_3 was found to be ~ 49 nm for x = 0.1 and ~ 45 nm for x = 0.2, 0.3. The unit cell parameters of pure as well as doped $BiFeO_3$ samples were calculated and their values have been tabulated in **Table 1**. It was observed that with increase in doping concentration, cell parameters and unit cell volume increase which might be attributed to substitution of greater ionic radius Sr^{2+} (1.26 Å) as compared to Bi^{3+} (1.17 Å).

Table 1. Unit cell parameters and volumes of all samples $Bi_{1-x}Sr_x$ FeO_3 (x = 0, 0.1, 0.2, 0.3).

Concentration x in $Bi_{1-x}Sr_x$	0.0	0.1	0.2	0.3
a (Å)	5.56644	5.57054	5.57484	5.57562
c (Å)	13.83936	13.84119	13.84882	13.85938
V ($Å^3$)	371.3655	371.9622	372.7419	373.1305

The XRD peak positions in Sr doped $BiFeO_3$ show slight variations in comparison with pure $BiFeO_3$. Enlarged view of the diffraction peaks for (012) and (104), (110) reflections around $2\theta=22.5^o$ and 32^o is shown in **Fig. 2(a)** and **2(b)** respectively. The replacement of Sr atoms (ionic radius ~1.26 Å) in place of Bi atoms having comparatively smaller ionic radius (~1.17 Å) results in slight shifting of all XRD peaks towards low angle which indicates an increase in lattice parameters [34]. Benfang Yu *et al* (2008) reported that shifting of peaks towards lower angles represent an increase in lattice parameters **[35]**. The shifting of (104) and (110) peaks towards lower 2θ values and reduced separation between these peaks (**Fig. 2**) indicate the distortion in the rhombohedral structure of $BiFeO_3$ without ensuing any structural transformation.

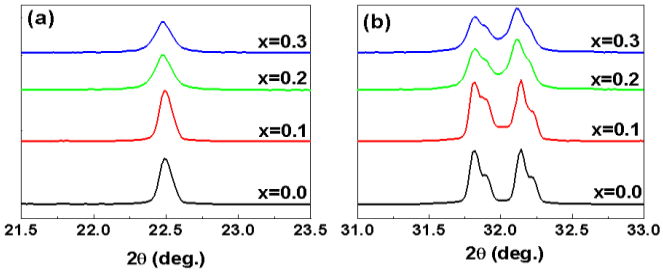

Fig. 2. Enlarged view of the diffraction peaks around (a) $2\theta=22.5^0$ and (b) 32^0

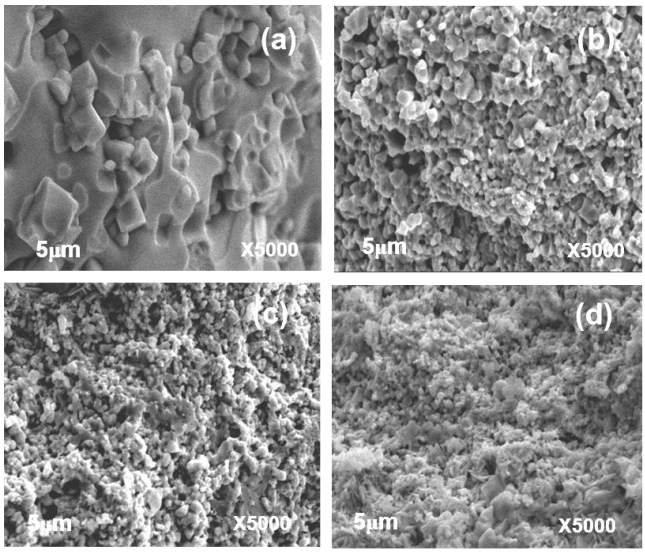

Fig. 3. SEM of fractured samples of $Bi_{1-x}Sr_x$ FeO_3: (a) x=0.0; (b) x = 0.1; (c) x= 0.2; (d) x = 0.3

The micro structural analysis of $Bi_{1-x}Sr_x$ FeO_3 (x = 0, 0.1, 0.2, 0.3) fractured pellet samples were carried out by using a scanning electron microscope (SEM) are shown in **Fig. 3**. The SEM image of pure $BiFeO_3$ sample reveals well defined sharp edged grains with varying sizes. However, with Sr doping the morphology of grains altogether changes and small sized grains were prevailing. The size of grains continues to decrease with increase in Sr doping (x = 0.10, 0.20 and 0.30). The fractured sample micrographs of all the samples also indicate that the decrease in the porosity of the samples with the increase in Sr doping. Most of the grains are homogeneous but a few grains of irregular shapes were also observed. The variation of grain morphologies may be an evidence of the formation of secondary phases. Larger grain size in pure $BiFeO_3$ may be due to evaporation of Bi which creates hefty number of oxygen vacancies and favours ion diffusion **[34]**. This provides an easy way out for the ions to diffuse, resulting in big sized grain as compared to the Sr doped $BiFeO_3$ samples. This phenomenon may decline due to replacement of Sr atoms (larger ionic radius) in place of Bi atoms (smaller ionic radius) and also grain growth may be inhibited by presence of phase $Bi_2Fe_4O_9$.

Magnetic Studies

Fig. 4 shows the variation of magnetization with an applied field (M-H studies) at room temperature for $BiFeO_3$ as well as for $Bi_{1-x}Sr_x$ FeO_3 (x = 0.1, 0.2, 0.3) samples. Pure $BiFeO_3$ shows a narrow hysteresis loop (shown in inset (i) of Fig. 4) indicating a weak ferromagnetism with remnant magnetization ~ $0.4x10^{-3}$ emu/g and coercive field ~ 0.065 kOe. Variation of Coercive Field and remnant magnetization with Sr doping in $Bi_{1-x}Sr_xFeO_3$ (x = 0, 0.1, 0.2, 0.3) has been shown in the inset (ii) of **Fig. 4**.

The value of magnetization has been found to increase with enhanced Sr doping having maximum value of M_r ~ 0.525 emu/g and H_c ~ 3.70 kOe for x = 0.30. In similar studies, enhanced magnetization has been reported in Ba, Ca, Sr, La doped $BiFeO_3$ **[37-39]**. In present studies, observed remnant magnetization and coercive field for Sr

doped $BiFeO_3$ is more than the reported values too best of our knowledge. With the increase in the content of divalent Sr ions at Bi-site in $BiFeO_3$, compensation of the charge of doped $BiFeO_3$ samples is favoured due to the possibility of the occurrence of some oxygen vacancies **[40-41]**. The average radius at Bi-site increases with the increase in Strontium content. This results in change in the interatomic distances and deviation of Fe – O – Fe bond angle from 180°. This bond angle controls the super exchange interaction between the anti-ferromagnetically aligned Fe^{3+} ions via the superseding oxygen anions. Ferromagnetic interactions dominate over anti-ferromagnetic interactions as Fe–O–Fe bond angle with Sr content. Therefore, the suppression of the spatially modulated spiral spin structure and thus the net magnetization might be induced due to the internal chemical pressure exerted due to Sr substitution. Oxygen vacancies may not be the only reason to augment the net magnetization of $Bi_{1-x}Sr_xFeO_3$ (x = 0.1, 0.2, 0.3) samples. A larger ionic radius of the doped element cause distortion that suppresses the spiral spin structure to break the inversion symmetry **[36]**. The increase in cell parameters, peak shift and reduced separation in peaks observed in XRD studies corroborates the distortion of structure. The spiral spin structure is changed into cycloid type structure that induced net magnetization in doped $BiFeO_3$ material. The observed crystallite size in doped samples being less than 62 nm may contribute to unlock the magnetization **[42-43]**. Wu *et al* (2013) has reported that nano-sized $Bi_2Fe_4O_9$ particles also contributed for enhancement in ferromagnetism **[44]**. Therefore, presence of nano-sized secondary phase $Bi_2Fe_4O_9$ particles in the compounds investigated in present paper showed improved multiferroic properties at room temperature.

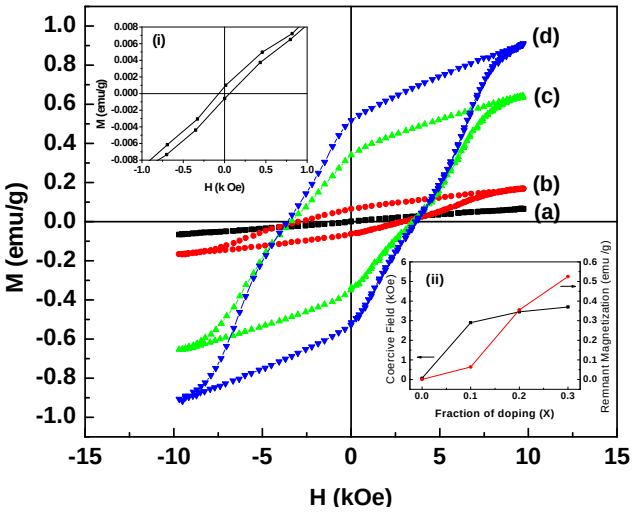

Fig. 4. Magnetization (M-H) loops for $Bi_{1-x}Sr_xFeO_3$: (a) x=0, (b) x= 0.1, (c) x= 0.2, (d) x= 0.3 at room temperature. The inset (i) shows an enlarged view of the loop for $BiFeO_3$ and inset (ii) shows the variation of Remnant magnetization and Coercive Field in $Bi_{1-x}Sr_x$ FeO_3 with Sr doping.

Leakage Current Studies

To investigate the leakage behaviour of the $Bi_{1-x}Sr_x$ FeO_3 (x = 0, 0.1, 0.2, 0.3) system, the leakage current densities were measured at room temperature by applying varying electric field up to 350 V/cm. **Fig. 5 (a),** demonstrated an increase in current density with increase in electric field for all samples. The doping of Sr (x =0.10) in $Bi_{1-x}Sr_x$ FeO_3 reduces its leakage current density up to three orders of magnitude as compared too pure $BiFeO_3$. With further increase in Sr concentration leakage current density increases. The lowest leakage current density for $Bi_{1-x}Sr_x$ FeO_3 (x = 0.10) confirms that it has fewer defects. Whereas the higher leakage current density for x = 0.20 and 0.30 doped $BiFeO_3$ might be due to more oxygen vacancies in their lattice. Higher leakage current may be attributed to existence of a multiphase and lattice in-homogeneity originated due to excess substitution of Sr for Bi **[4]**. However, the large leakage current in case of pure $BiFeO_3$ is attributed to large grain microstructures as compared to that in doped samples **[34]**.

The plots showing logarithmic variation of the current density, 'J' and electric field, 'E' is highly useful to uncover the mechanism involved in the leakage behaviour of the samples. Based on the power law $J \alpha E^s$ relationship [45], log (J) versus log (E) was plotted in **Fig. 5(b)** for $Bi_{1-x}Sr_x$ FeO_3 (x=0, 0.1, 0.2, 0.3). The conduction mechanism involved in a specific region of these curves can be estimated from the value of slope of that region **[45]**. The estimated value of slope is found to be less than unity for all the samples in the low electric field region indicating conduction being limited by grain boundary. The estimated value of slope is greater than 1 (s > 1) in the regions of high electric field, which shows emergence of space-charge-limited conduction (SCLC) **[45]**. However, in case of x = 0.10 doped $BiFeO_3$ space-charge-limited conduction (SCLC) starts at comparatively higher field values. Lesser amount of secondary phase and oxygen vacancies leading to lesser concentration of charge defects might be attributed for this behaviour.

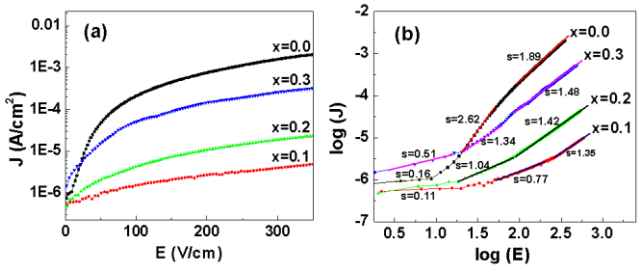

Fig. 5. (a) Leakage current density, J vs. Electric Field, E for the samples $Bi_{1-x}Sr_xFeO_3$ (x = 0, 0.1, 0.2, 0.3), (b) log (J) vs. log (E) plot for the samples $Bi_{1-x}Sr_xFeO_3$ (x = 0, 0.1, 0.2, 0.3).

Ferroelectric Studies

The ferroelectric hysteresis loop (P-E) measurement is always held back by presence of defects and oxygen vacancies that make it very hard to get good ferroelectric properties in $BiFeO_3$ ceramics. The P-E loops at room temperature for $Bi_{1-x}Sr_x$ FeO_3 (x=0, 0.1, 0.2, 0.3) have been shown in **Fig. 6**. The $BiFeO_3$ displays an unsaturated hysteresis loop which is rounded at the maximum field regions. Due to the poor leakage behaviour saturated polarization–electric field (P–E) curve could not be obtained for the $BiFeO_3$ up to the maximum applied electric field. This implies highly conductive nature of the samples at room temperature and indicates only partial reversal of

the dipoles **[33]**. The changeable oxidation states of Fe ions (Fe^{+2} to Fe^{+3}) via oxygen vacancies occurring from charge compensation is known to be ascribed for relatively high conductivity of $BiFeO_3$. In spite of ferroelectric nature of $BiFeO_3$, the actual contribution from reorientation of electrical dipoles is overshadowed by large leakage current and lossy hysteresis loops are observed. The doped $Bi_{1-x}Sr_xFeO_3$ (x = 0.1, 0.2, 0.3) samples exhibit a smaller polarization compared to the $BiFeO_3$ parent compound. It suggests that the leakage current is less in doped compound compared to the pure one.

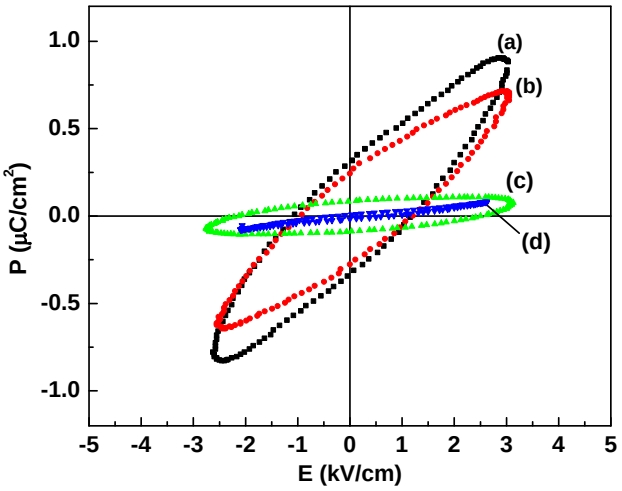

Fig. 6. P-E curves for $Bi_{1-x}Sr_xFeO_3$: (a) x=0, (b) x= 0.1, (c) x = 0.2, (d) x= 0.3 at room temperature.

Conclusion

$Bi_{1-x}Sr_xFeO_3$ (x=0, 0.1, 0.2, 0.3) were successfully synthesized using combustion method. Traces of $Bi_2Fe_4O_9$ phase of bismuth ferrite was also observed in all Sr-doped samples. The size of the crystallite remained nearly invariable with Sr doping. The increase in lattice parameters with increased substitution of Sr at Bi-site results in structural distortion. The morphological study of the samples using SEM revealed the decrease in size of grains with increase in the Sr-contents in $BiFeO_3$. The magnetic hysteresis loops exhibit enhanced magnetization in $Bi_{1-x}Sr_xFeO_3$ (x = 0.1, 0.2, 0.3) samples at room temperature. Doped samples showed smaller leakage current than that of pure $BiFeO_3$ which improves its multiferroic properties to significant extent.

Acknowledgements

The authors acknowledge I.K. Gujral Punjab Techncial University, Kapurthala for providing research facilities. The authors are also grateful to Sophisticated Analytical Instrumentation Facility, Panjab University, Chandigarh for providing X-Ray Diffraction facility. In addition, the first author acknowledges University Grant Commission (UGC), New Delhi for providing teacher fellowship and parent organization Punjabi University Patiala, Punjab (India) for granting study leave to pursue research work.

References

1. Spaldin, N. A.; Cheong, S. W.; and Ramesh, R.; *Phys. Today.*, **2010**, *63*, 38. **DOI:** http://dx.doi.org/10.1063/1.3502547
2. Khomskii, D.; *Physics. 2*, **2009,** *20***,** 8. **DOI:** link.aps.org/doi/10.1103/Physics.2.20
3. Catalan, G; Scott, J. F.; *Adv. Mater.*, **2009,** *21*, 2463. **DOI:** 10.1002/adma.200802849
4. Xu, X.; Guoqiangn .; Huijun ,R.; Ao, X.; *Ceram. Int.*, **2013**, *39***,** 6223. **DOI:** 10.1016/j.ceramint.2013.01.042
5. Bea, H.; Gajek, M.; Bibes, M.;and Barthelemy, A.; *J. Phys. Condens. Matter*. **2008**, *20*, 434221. **DOI:** 10.1088/0953-8984/20/43/434221
6. Bibes, M.; and Barthelemy, A.; *Nat. Mater.*, **2008**, *7***,** 425. **DOI:** 10.1038/nmat2189
7. Hussain, T.; Siddiqi, S. A.; Atiq, S.; Awan, M. S; *Prog. Nat. Sci.: Mater.*, **2013**, *23***,** 487. **DOI:** 10.1016/j.pnsc.2013.09.004
8. Bhushan, B.; Basumallick, A.; Bandopadhyay, S. K.; Vasanthacharya, N. Y.; and Das D.; J. *Phys. D: Appl. Phys.*, **2009,** *42*, 065004. **DOI:** 10.1088/0022-3727/42/6/065004
9. Azam, A.; Jawad, A.; Ahmed, A. S.; Chaman, M.; Naqvi, A. H.; *J Alloys Compd.*, **2011**, *509***,** 2909. **DOI:** 10.1016/j.jallcom.2010.11.153
10. Scott, J. F.; *Nat. Mater.*, **2007**, 6, 256. **DOI:** 10.1038/nmat1868
11. Zhou, Y.; Fang, L.; You, L.; Ren, P.; Wang, L.; Wang, J.; *Appl. Phys. Lett.*, **2014**, *105*, 252903. **DOI:** 10.1063/1.4905000
12. Wang, J.; Zheng, H.; Ma, Z.; Prasertchoung, S.; Wuttig, M.; Droopad, R.; Yu, J.; Eisenbeiser, K.; Ramesh R.; *Appl. Phys. Lett.*, **2004**, *85*, 2574. **DOI:** 10.1063/1.1799234
13. Belik, A. A.; Furubayashi, T.; Matsushita, Y.; Tanaka, M.; Hishita, S.; Muromachi, E. T.; *Angew. Chem. Int. Ed.*, **2009**, *48*, 6117. **DOI:** 10.1002/anie.200902827
14. Xu, Q,.; Zai, H.; Wu, D.; Qiu, T.; and Xu, M .X.; *Appl. Phys. Lett.*, **2009**, 95, 112510. **DOI:** http://dx.doi.org/10.1063/1.3233944
15. Liu, J.; Fang, L.; Zheng, F.; Ju, S.; Shen, M.; *Appl. Phys. Lett.*, **2009**, *95*, 022511. **DOI:** http://dx.doi.org/10.1063/1.3183580
16. Khomchenko, V. A.; Kiselev. D. A.; Vieira, J. M.; Kholkin, A. L.; Sa, M. A.; Pogorelov, Y. G.; *Appl. Phys. Lett.*, **2007**, *90*, 242901. **DOI:** http://dx.doi.org/10.1063/1.2747665
17. Kawae, T.; Terauchi, Y.; Tsuda, H.; Kumeda, M.; Morimoto, A.; *Appl. Phys. Lett* , **2009**, *94*, 112904. **DOI:** http://dx.doi.org/10.1063/1.3098408
18. Kothari, D.; Reddy, V. R.; Gupta, A.; Sathe, V.; Banerjee, A.; Gupta, S. M.; and Awasthi, A. M.; *Appl. Phys. Lett.* **2006**, *91***,** 202505. **DOI:** http://dx.doi.org/10.1063/1.2806199
19. Wang, D. H.; Goh, W. C.; Ning, M.; and Ong, C. K.; Appl. *Phys. Lett.*, **2006**, *88*, 212907. **DOI:** http://dx.doi.org/10.1063/1.2208266
20. Biswal, .M. R. Nanda, J.; Mishra, N. C.; Anwar, S.; Mishra, A.; *Adv. Mater. Lett.*, **2014**, *5 (9)***,** 531. **DOI:** 10.5185/amlett.2014.5666
21. Li, J. B.; Rao, G. H.; Liang, J. K.; Liu, Y. H.; Luo, J.; and Chen, J. R.; *Appl. Phys. Lett.*, **2007**, *90*, 162513. **DOI:** http://dx.doi.org/10.1063/1.2720349
22. Wei, J.; Haumont, R.; Jarrier, R.; Berhtet, P.; and Dkhil, B.; *Appl. Phys. Lett.* , **2010**, *96*, 102509. **DOI:** http://dx.doi.org/10.1063/1.3327885
23. Selbach, S. M.; Tybell, T.; Einarsrud, M. A.; and Grande, T.; *Chem. Mater.*, **2007**, *19*, 6478. **DOI:** 10.1021/cm071827w
24. Jaiswal, A.; Das. R.; Vivekanand, K.; Abraham, P. M.; Adyanthaya, S.; and Poddar, P.; *J. Phys. Chem. C*, **2010**, *114***,** 2108. **DOI:** http://dx.doi.org/10.1021/jp910745g
25. Bai, F.; Wang, J.; Wuttig, M.; Li, J.; Wang, N.; Pyatakov, A. P.; Zvezdin, A. K.; Cross, L. E.; and Viehland, D.; *Appl. Phys. Lett.*, **2005**, *86***,** 032511 **DOI:** http://dx.doi.org/10.1063/1.1851612
26. Reddy, V. A.; Sekhar, K. C.; Dabra, N.; Nautiyal, A.; Hundal, J. S.; Pathak, N. P.; and Nath, R.; *ISRN Mater. Sci.*, **2011** Article ID 142968, 5 pages **DOI:** http://dx.doi.org/10.5402/2011/142968

27. Redd,y .V A. Dabra, N.; Hundal, J. S.; Pathak, N. P.; and Nath, R.; *Sci. Adv. Mater.*, **2014,** *6***,** 1228. **DOI:** http://dx.doi.org/10.1166/sam.2014.1922
28. Wang, J. et al; *Science*, 2003**,** *299***,** 1719. **DOI:** 10.1126/science.108061
29. Layek, S.; Verma, H. C.; *Adv. Mat. Lett*,. **2012**, *3*, 533. **DOI:** 10.5185/amlett.2012.icnano.242
30. Jain, S. R.; Adiga, K. C.; Pai Verneker, V. R.; *Combust. Flame*, **1981**, *40*, 71. **DOI:** 10.1016/0010-2180(81)90111-5
31. Patil, K. C.; Hegde, M. S.; Rattan, T.; Aruna, S.T.; Chemistry of Nanocrystalline Oxide Materials; Singapore, World Scientific Publishing Co. Pte. Ltd. **2008**.
32. JCPDS International Centre for Diffraction Data, **1998**; File No. 03-0628.
33. Teague, J. R.; Gerson, R.; James, W. J.; *Solid State Comm.*,**1970**, *8*, 1073. **DOI:** 10.1016/0038-1098(70)90262-0
34. Makhdoom, A. R.; Akhtar, M. J.; Rafiq, M. A.; Hassan, M. M.; *Ceram. Int.*, 2012, 38, 3829. **DOI:** 10.1016/j.ceramint.2012.01.032
35. Yu, B.; Li, M.; Liu, J.; Guo, D.; Pei, L.; and Zhao, X.; *J. Phys. D: Appl. Phys*., **2008,** *41***,** 065003. **DOI:** 10.1088/0022-3727/41/6/065003
36. Paul Khomchenko, V. A.; et al , *J. Magn. Magn. Mater.*, **2009**, *321*, 1692. **DOI:** 10.1016/j.jmmm.2009.02.008
37. Blessington Selvadurai , A.; Pazhanivelu, V.; Murugaraj, R.; *J. Supercond. Nov. Magn.*, **2014**, *27*, 839. **DOI:** 10.1007/s10948-013-2349-3
38. Rangi, M.; Agarwal, A.; Sanghi, S.; Singh, R.; Meena, S.S.; and Das, A.; *AIP Adv.*, **2014**, *4*, 087121. **DOI:** http://dx.doi.org/10.1063/1.4893241
39. Reddy, V. Annapu,.; Dabra, N.; Ashish, K.K.; Hundal, Jasbir S.; Pathak, N. P,.; and Nath, R,. Adv. Mater. Lett., **2015**, 6(8), 678. **DOI:** 10.5185/amlett.2015.5802
40. Singh, P.; Jung, J. H.; *Physica B*, **2010**, *405*, 1086. **DOI:** 10.1016/j.physb.2009.11.007
41. Bhushan, B.; Basumallick, A.; Vasanthacharya, N. Y.; Kumar, S.; and Das, D.; *Solid State Sci.*, **2010**, *12*, 1063. **DOI:** 10.1016/j.solidstatesciences.2010.04.026
42. Park, T. J.; Papaefthymiou, G. C.; Viescas, A. J.; Moodenbaugh, A. R.; and Wong, S. S.; Nano *Lett*. **2007**, *7*, 7766. **DOI:** 10.1021/nl063039w
43. Jie, W.; Jun, C. Y.; Zhuo, X.; *Acta Phys. Sin.*, **2012**, *61*, 057502. **DOI:** 10.7498/aps.61.057502
44. Wu, X. H.; Miao, J.; Zhao, Y ; Meng, X. B.; Xu, X. G.; Wang, S. G.; Jiang, Y.; *Optoelectron. Adv. Mat.* , **2013**, *7*, 116.
45. Qi, X.; Dho, J.; Tomov, R.; Blamire, M. G.; and MacManus-Driscoll, J. L.; *Appl. Phys. Lett.*, **2005**, *86***,** 062903. **DOI:** http://dx.doi.org/10.1063/1.1862336

